

Curvature vs Distances: testing the FLRW cosmology

Domenico Sapone,^{*} Elisabetta Majerotto,[†] and Savvas Nesseris[‡]
*Departamento de Física Teórica and Instituto de Física Teórica,
Universidad Autónoma de Madrid IFT-UAM/CSIC,
28049 Cantoblanco, Madrid, Spain*

We test the FLRW cosmology by reconstructing in a model-independent way both the Hubble parameter $H(z)$ and the comoving distance $D(z)$ via the most recent Hubble and Supernovae Ia data. In particular we use: data binning with direct error propagation, the principal component analysis, the genetic algorithms and the Padé approximation. Using our reconstructions we evaluate the Clarkson *et al* test known as $\Omega_K(z)$, whose value is constant in redshift for the standard cosmological model, but deviates otherwise. We find good agreement with the expected values of the standard cosmological model within the experimental errors. Finally, we provide forecasts, exploiting the Baryon Acoustic Oscillations measurements from the Euclid survey.

PACS numbers: 95.36.+x, 98.80.-k, 98.80.Es

I. INTRODUCTION

The observed accelerated expansion of the late-time universe, as evidenced by a number of cosmological data like type Ia supernovae (SnIa) [1], the cosmic microwave background radiation [2] (CMB) and large scale structure [3] (LSS) came as a great surprise to cosmologists. It is quite straightforward to explain the effect within the framework of Friedmann-Lemaître-Robertson-Walker (FLRW) cosmology by simply introducing a cosmological constant or a more general (dynamical) dark energy component. However, all such components give rise to severe coincidence and fine-tuning problems. An alternative approach postulates that General Relativity is only accurate on small scales and modifications at larger scales are needed. These modification would lead to the observed late-time acceleration [4–7].

Recently, several works have tried to take a different approach, namely to study the effect of large scale structure on the observed luminosity-to-redshift behavior of SnIa (the first observable that has led to the conclusion that the Universe is accelerating). The assumption that the Universe is homogeneous and isotropic is known to be violated at late times. However, the scale at which the assumption breaks down is still in debate, [8]. Nonetheless, recent studies have been able to reproduce the luminosity-to-redshift relation provided that we live in a large region, called empty void, in which the matter density is less than the spatial average density on large cosmological scales ([9], for a recent review see [10]). However, also these models are still in debate since they require the observer to be located at the center of the void or at most within about few percent of the void scale radius [11], thus disfavoring the model from a Copernican Principle (CP) point of view.

Despite all the theoretical efforts to understand the accelerated expansion of the Universe, see [12, 13], right now there is no model capable of providing singlehandedly a satisfactory explanation. An alternative is to create null tests for the current paradigm and see if and how it breaks down. For example, Clarkson *et al.* [14] presented a new test for the CP which relies on a consistency relation that exists within the homogenous and isotropic FLRW model between the luminosity and the Hubble parameter. This relation is expected to hold exactly at all redshifts z , and any deviation will point to a departure from the FLRW model. Indeed, to be precise, the test of Clarkson *et al.* tests deviations from a FLRW metric and not strictly from the CP, as pointed out by [15–17].

The existence of this consistency relation implies that if we have two separate experiments measuring independently the comoving distance $D(z)$ (or equivalently the angular diameter distance or the luminosity distance) and the Hubble parameter $H(z)$, then we are able to reconstruct the curvature parameter Ω_K at each redshift in a model-independent way. In a FLRW universe, the curvature parameter should not depend on redshift, hence Ω_K should not vary, so if we measure a variation of the curvature parameter over redshift, this means that the assumption of homogeneity at large scales has to be rejected.

Since it was proposed, this test has raised interest in the astrophysics community. Ref. [18, 19] have applied it by using available data; ref. [20] has discussed the deviation from the FLRW relation due to backreaction; refs.

^{*}Electronic address: domenico.sapone@uam.es

[†]Electronic address: elisabetta.majerotto@uam.es

[‡]Electronic address: savvas.nesseris@uam.es

[16, 21–23] have predicted the outcome of the test, i.e. the behavior of Ω_K with redshift, in the case of their particular inhomogeneous cosmology or void model; ref. [24] has made predictions on future results from the test if a toy-model of backreaction is assumed to be the correct cosmology; ref. [25] has used it to measure the curvature of the Universe in a model-independent way. Also, many other tests of the standard model of cosmology have been outlined (for most recent work, see [26], and for a review see [27, 28])

In particular, ref. [18] has used $H(z)$ data from passively evolving galaxies [29, 30] and the SnIa of [31] and has found no indication of a deviation from FLRW. Ref. [25] has used SnIa data of [32], $H(z)$ data from passively evolving galaxies [33] and baryonic acoustic oscillation (BAO) data [34], and the H_0 measurement of [35]. Similarly, ref. [19] has used the SnIa of [36] and the measurement of H_0 of [35] or of [37], in combination with $H(z)$ measurements coming either from passively evolving galaxies [29, 33], or from BAO data [38], together with cosmic microwave background data [39]. No evidence for deviations from FLRW nor from flatness was found.

In this context, our work has two objectives, building on the work of [19] and [24]. The first objective is to improve the measurement of Ω_K by comparing four different measurement techniques based both on binnings of the data and on very efficient model-independent reconstructions of functions, and by using the most recent data. The second is to make new up-to-date forecasts for the Ω_K test for future LSS and SnIa data.

The paper is organized as follows: in Sec. II we describe the general background equations used for our analysis. In Sec. III we describe four different methods to reconstruct the Hubble parameter and the comoving distance from two different data sets. In particular we show: the data binning and direct error propagation method, the principal component analysis (PCA), the genetical algorithms (GA) and the Padé approximation. In each subsection we report the results. Sec. IV is devoted to the Fisher matrix forecasts on the errors for the Ω_K at different z using the Euclid galaxy redshift survey¹ [40, 41] and future SnIa surveys.

II. BACKGROUND EQUATIONS

Here we review the basic equations and notation for the background evolution. The evolution of the dark energy can be expressed by the present dark energy density Ω_{DE} and by a time-varying equation of state:

$$w(z) = \frac{p}{\rho}. \quad (1)$$

Where p and ρ are the pressure and energy density of dark energy, respectively. The dark energy density equation is $\rho(z) = \rho(0)a^{-3(1+\hat{w})}$ and

$$\hat{w}(z) = \frac{1}{\log(1+z)} \int_0^z \frac{w(z')}{1+z'} dz'. \quad (2)$$

The Hubble parameter $H(z)$ and the angular diameter distance $D_A(z)$, in a flat universe with $\Omega_m + \Omega_{DE} = 1$, are

$$H^2(z) = H_0^2[\Omega_m(1+z)^3 + (1-\Omega_m)(1+z)^{3(1+\hat{w})}] \quad (3)$$

and

$$D_A(z) = \frac{c}{1+z} \int_0^z \frac{dz}{H(z)}. \quad (4)$$

In a general FLRW model with curvature, the angular diameter distance can be written as:

$$D_A(z) = \frac{c}{1+z} \frac{1}{H_0 \sqrt{-\Omega_K}} \sin \left(\sqrt{-\Omega_K} \int_0^z dz' \frac{H_0}{H(z')} \right). \quad (5)$$

where Ω_K is the curvature parameter today.

We can invert Eq. (5) to obtain an expression for the curvature parameter Ω_K that depends on the Hubble parameter $H(z)$ and comoving distance $D(z) = (1+z)D_A(z)$, see [14]:

$$\Omega_K(z) = \frac{[H(z)D_{,z}(z)]^2 - 1}{[H_0 D(z)]^2}, \quad (6)$$

¹ <http://www.euclid-ec.org/>

where the comma refers to the derivative with respect to the redshift. The above equation tells us how we can measure the curvature parameter in a model-independent way from Hubble rate and distance measurements. If we live in a FLRW universe, then the curvature parameter is independent of redshift, i.e. $\Omega_K(z)$ should be a constant $\Omega_K(z) = \Omega_K$; however, if we measure a variation of the curvature parameter, this would indicate that the homogeneity of the large-scale universe is violated.

In order to test the values of Ω_K at different redshifts we need to combine two independent measurements: that of the Hubble parameter $H(z)$ and that of the comoving distance $D(z)$. In the next section we will use the Hubble parameter data set from [42] and the SnIa magnitude data-set from the SCP “Union2.1” [43, 44] to reconstruct the curvature parameter as a function of redshift.

III. RECONSTRUCTING $H(z)$ AND $D(z)$

In this section we present four different ways to reconstruct the curvature parameter using measurements of the Hubble parameter and comoving distance from SnIa.

A. Data sets

First, we briefly describe the data sets that we will use in the present analysis. These are:

- The Hubble parameter data that directly probe $H(z)$, in the most recent compilation given by Moresco et al. [42]. The authors implemented a *differential approach* to evaluate the Hubble parameter; first they chose from different catalogs early-type galaxies and then they selected only the most massive, red elliptical galaxies which are passively evolving and do not manifest any signature of ongoing star formation. The Hubble parameter is then given by

$$H(z) = -\frac{1}{1+z} \frac{dz}{dt} \quad (7)$$

where dz is simply given by the difference in redshift of two galaxies and dt is given by their differential dating of star populations.

- The SnIa data that probe the luminosity distance $d_L(z) \equiv (1+z)D(z)$, where $D(z)$ is the comoving distance. In particular, we use the “Union2.1” set of 580 SnIa of Suzuki et al. [44]². The data are given in terms of the distance modulus

$$\mu(z) \equiv m(z) - M = 5 \log_{10}(d_L(z)) + 25 \quad (8)$$

$$= 5 \log_{10}(H_0 d_L(z)) + \mu_0, \quad (9)$$

where $m(z)$ is the apparent magnitude at peak brightness, M is the absolute magnitude and $\mu_0 = 42.38 - 5 \log_{10} h$ with $h = H_0/[100 \text{ km sec}^{-1} \text{ Mpc}^{-1}]$. The chi-square is then

$$\chi_{SnIa}^2 = \sum_{i=1}^{580} \left(\frac{\mu_{obs}(z_i) - \mu_{th}(z_i)}{\sigma_i} \right)^2. \quad (10)$$

For simplicity we only consider the case where the covariance matrix of the SnIa data is diagonal.

B. Binning SnIa and $H(z)$ data

The first technique to measure $\Omega_K(z)$ consists in evaluating it in several redshift bins by directly computing the comoving distance $D(z)$ and its derivative $D_{,z}$ from the SnIa data and by using the $H(z)$ values measured from

² The SnIa data can be found in <http://supernova.lbl.gov/Union/> and in [44]

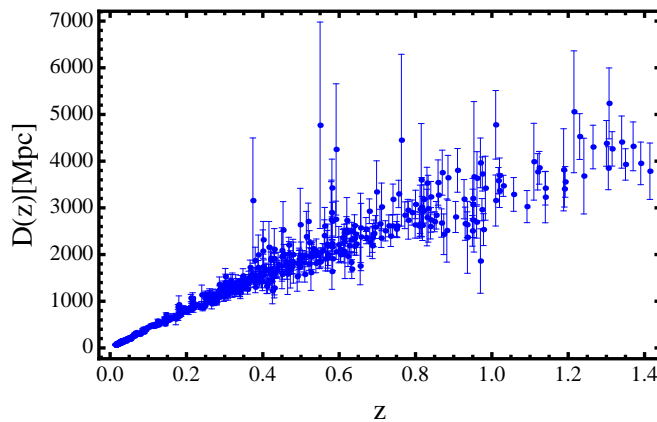


Figure 1: Comoving distances computed directly from the 580 SnIa of the “Union2.1” compilation [43] by using Eq. (11).

Bins	z_{min}	z_{max}	z_H	\bar{z}	# of SnIa	# of H(z)	\bar{D}	$D_{,z}$	Ω_K
1	0.00	0.13	0.09	0.044	194	1	114.29 ± 0.68	4578 ± 71	138 ± 490
2	0.13	0.17	0.17	0.16	20	1	622.9 ± 7.7	2892 ± 1068	-15 ± 21
3	0.17	0.19	0.18	0.18	12	1	750 ± 14	-12036 ± 8445	237 ± 375
4	0.19	0.23	0.20	0.21	24	1	864 ± 11	2375 ± 1296	-14.3 ± 8.6
5	0.23	0.31	0.27	0.27	54	1	1075 ± 11	3719 ± 601	-1.3 ± 6.3
6	0.31	0.38	0.35	0.34	37	1	1340 ± 18	4821 ± 1407	7 ± 11
7	0.38	0.44	0.40	0.41	43	1	1589 ± 25	4581 ± 1505	7 ± 10
8	0.44	0.54	0.48	0.49	43	1	1858 ± 28	2713 ± 1190	-1.1 ± 5.7
9	0.54	0.64	0.59	0.59	45	1	2076 ± 29	3189 ± 1233	0.9 ± 3.8
10	0.64	0.73	0.68	0.68	23	1	2429 ± 52	1980 ± 2266	-1.8 ± 2.4
11	0.73	0.83	0.78	0.79	22	1	2775 ± 61	2181 ± 2262	-0.9 ± 2.6
12	0.97	1.17	1.04	1.04	19	1	3370 ± 85	1143 ± 1591	-1.0 ± 1.4
13	1.17	1.37	1.30	1.26	13	1	4018 ± 131	2616 ± 2754	1.2 ± 4.6

Table I: Properties of bins described in Sec. IIIB1 and values of the comoving distance \bar{D} , derivative of the comoving distance $D_{,z}$ and curvature parameter Ω_K measured in each bin. With z_{min} and z_{max} we indicate the left and right edge of each bin, respectively. z_H refers to the redshift to which the mean distance \bar{D} has been assigned, while \bar{z} is the mean redshift of the bin.

passively evolving galaxies data. To compute $D(z)$, we simply invert Eq. (9) that expresses the distance modulus μ as a function of $D(z)$:

$$D(z) = \frac{10^{\frac{\mu-25}{5}}}{1+z}. \quad (11)$$

The resulting comoving distances computed from the “Union2.1” SnIa are shown in Fig. 1. The obtained data are then divided into bins. We do this in two different ways, in order to understand which way produces the best results, and to control the dependence on the specific binning.

1. First binning criterion

In the first approach, we aim at maximising the number of bins. Since the number $n_H = 19$ of $H(z)$ data is quite small, we choose a number of bins as close as possible to n_H . To do so, we use the following procedure. We split the redshift interval $\Delta z_{i,i+1}$ between each pair of $H(z)$ data, $H(z_i)$ and $H(z_{i+1})$, into two equal parts. We take $z = 0$ as the initial redshift of the first bin. Since the SnIa’s highest redshift is $z = 1.414$, the last bin does not contain any SnIa, and we discard it. This means that we also have to discard the last two $H(z)$ data points. The resulting bins are given in Tab. I. In each bin we then compute the comoving distance \bar{D} as the weighted mean of the different D_i s contained in the bin, weighted by the square of the error on D_i , σ_i^2 , and assign \bar{D} to the redshift z_H . In principle, we

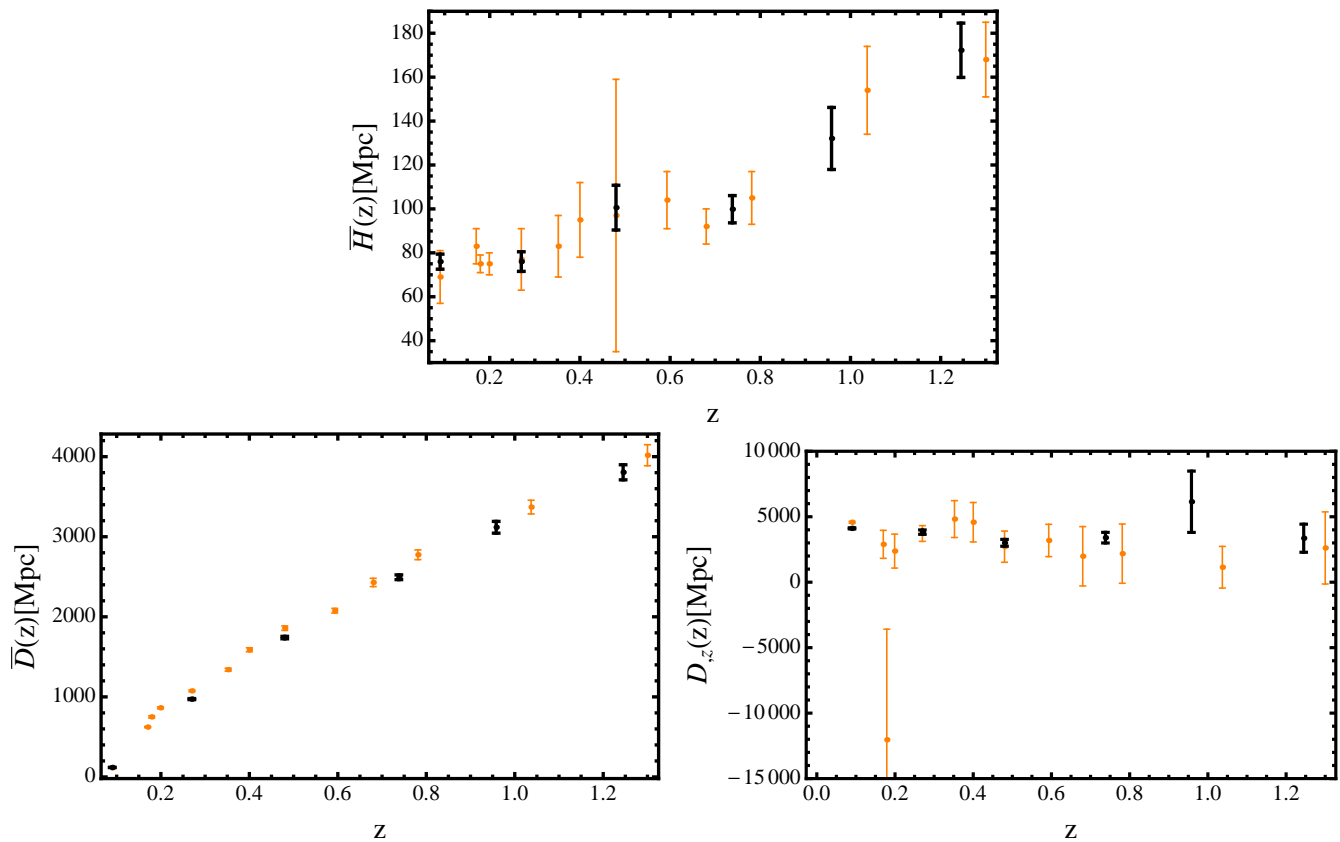


Figure 2: The mean Hubble function \bar{H} , comoving distance \bar{D} , and derivative of the comoving distance $D_{,z}$ computed with the binning of Secs. III B 1 (orange thin error bars) and III B 2 (black thick error bars). We omit to show horizontal error bars in order not to make the plot too crowded and confusing.

should assign \bar{D} to the mean redshift \bar{z} of each bin, but, as can be seen from Table I, \bar{z} and z_H are very close: only for the first bin the difference is larger than 9%, but here we will see that errors on Ω_K are extremely large anyway and constraints on Ω_K will not be useful in practice. The error on \bar{D} is then $\sigma_{\bar{D}} = 1/\sqrt{\sum_i 1/\sigma_i^2}$. To compute the derivative $D_{,z}$ we use one of the formulas for its discrete approximation:

$$D_{,z}(z) \simeq \frac{D(z + \Delta z_1) - D(z - \Delta z_2)}{\Delta z_1 + \Delta z_2}. \quad (12)$$

In order to apply this formula to our data, we split each bin into two parts, taking z_H as splitting point. We then compute \bar{D} in each sub-bin, obtaining two mean distances \bar{D}_{left} and \bar{D}_{right} . We assign \bar{D}_{left} and \bar{D}_{right} to the average redshift of the corresponding sub-bin, \bar{z}_{left} and \bar{z}_{right} , and finally compute the (approximated) derivative as

$$D_{,z}(z_H) = \frac{\bar{D}(\bar{z}_{right}) - \bar{D}(\bar{z}_{left})}{\bar{z}_{right} - \bar{z}_{left}}. \quad (13)$$

The error on the derivatives is obtained via the simple propagation of errors formula. We find that not all sub-bins contain at least one SNIa, so we eliminate from the sample all bins which have no SNIa in either the left or the right corresponding sub-bin. This leaves us with only 13 bins; as a consequence, only 13 out of 19 $H(z)$ data points and only 549 out of 580 SNIa data points are used. In Fig. 2 we show (orange thin error bars) \bar{H} , \bar{D} and $D_{,z}$ obtained with this binning.

We then compute $\Omega_K(z_H)$ at each redshift z_H by using Eq. (6), where, as already said, $D(z_H)$ and $D_{,z}(z_H)$ are computed from SNIa data as explained above, $H(z_H)$ come from passively evolving galaxies data and where we use $H_0 = 73.8 \pm 2.4$, as measured from the Hubble Space Telescope (HST) and the Wide Field Camera 3 [45].

The resulting Ω_K are shown in Fig. 3. We notice from the left panel of Fig. 3 that at the smallest and third smallest redshift the error bars are extremely large. Errors reduce noticeably for redshifts $z > 0.2$, and, for a better visualisation, on the right panel we focus on the region inside the yellow dashed box: $0.12 < z < 1.3$. Here we see that

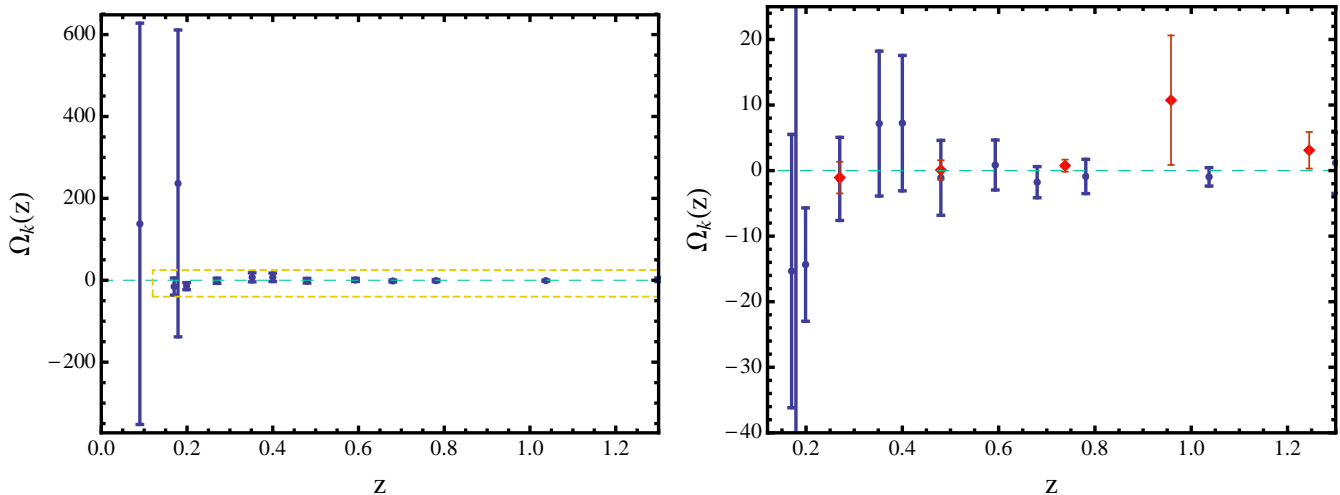


Figure 3: The curvature parameter Ω_K obtained by using $H(z)$ data from passively evolving galaxies and SnIa data and applying to them the binning procedure described in Sec. III B 1. For comparison, we also show results from the second binning procedure, described in Sec. III B 2, as red thin error bars. The light-blue long-dashed line corresponds to the case of a flat FLRW universe: $\Omega_K(z) = 0$. On the left panel we show our full results, while on the right panel we focus on the region inside the yellow dashed box, i.e. on redshifts where constraints are best: $z > 0.12$. We omit to show horizontal error bars in order not to make the plot too crowded and confusing.

the best constrained Ω_K ($\sigma_{\Omega_K} = 1.40$) is at $z = 1.04$, while at $z = 0.2$ the relative error is smallest: $\sigma_{\Omega_K}/|\Omega_K| = 0.60$. However, the smallness of the error at $z = 1.04$ is only apparent and due to the strongly fluctuating D_i close to this redshift, as can be seen from Fig. 1. We will comment more extensively on this in the following section.

A point to understand is the sensitivity to a particular choice of H_0 . From Eq. (6) we see that $\Omega_K \propto 1/H_0^2$. When changing e.g. from HST data to the Planck constraint [46] $H_0 = 67.3 \pm 1.2$, this results in a relative change in Ω_K of 18%. Since errors on Ω_K are $\geq 60\%$, and since they depend very little on the error on H_0 (errors differ by less than 0.4% if the error is halved) this does not affect our results. In the future however, it will be important for this test to be effective, that different measurements of H_0 give more compatible results.

Since errors are very large when using this binning system, we try a different one in the hope of improving our results.

2. Second binning criterion

This second criterion aims at maximizing the use of all available data. It uses the full SnIa set, and leaves out only two of the $H(z)$ data. We divide the redshift interval into 6 bins delimited by the following redshifts: $z = \{0, 0.18, 0.36, 0.6, 0.876, 1.04, 1.45\}$. The latter choice was made for two main reasons. First, we want to have at least two $H(z)$ data points in each bin. Second, we do not want to have bins that are too large, in order for the assumption that D and $H(z)$ be constant inside each bin to be still reasonable. Since we need to use the same binning for both datasets, the last two $H(z)$ data points have to be left out again. This is somehow inevitable as the two data-sets have different redshift ranges. We show the properties of the bins described above in Tab. II.

We then use the following procedure. First, we compute the weighted average distance, \bar{D} , and weighted average Hubble function, \bar{H} , in each bin. We assign these values to the redshifts at the centre of the bin, i.e. $z_i = \{0.09, 0.27, 0.48, 0.738, 0.958, 1.245\}$. Also here we should in principle assign \bar{D} to the mean redshift \bar{z} of each bin, but here, too, the difference between \bar{z} and z_i is very small (see Tab. II) except for the first bin, and the error we commit is very small. To compute $D_{,z}(z_i)$, we divide the Δz of each bin in two equal sub-bins and compute the weighted average distance in each sub-bin, obtaining two distances: \bar{D}_{left} and \bar{D}_{right} . We assign \bar{D}_{left} and \bar{D}_{right} to the average redshift of the corresponding sub-bin, \bar{z}_{left} and \bar{z}_{right} . We then use Eq. (13) to compute $D_{,z}(z_i)$. Fig. 2 shows as black thick error bars the values of \bar{H} , \bar{D} and $D_{,z}$ computed with this binning.

We finally compute $\Omega_K(z_i)$ by using Eq. (6). The results are shown in Fig. 4. We notice, by looking at the left panel, that also in this case the error bar of the lowest redshift point is very large. We will see in the following sections that this is a common feature of Eq. (6), and we will give an explanation for it in the conclusions. On the right panel we focus on the region corresponding to the yellow dashed box. We can see that the best absolute error ($\sigma_{\Omega_K} = 1.48$)

Bins	z_{min}	z_{max}	z_i	\bar{z}	# of SnIa	# of H(z)	\bar{D}	$D_{,z}$	Ω_K
1	0.00	0.18	0.09	0.057	218	3	118.59 ± 0.68	4113 ± 44	100 ± 118
2	0.18	0.36	0.27	0.27	115	3	972.3 ± 6.6	3824 ± 168	-1.1 ± 2.4
3	0.36	0.60	0.48	0.47	123	3	1741 ± 15	3008 ± 406	0.1 ± 1.5
4	0.60	0.88	0.74	0.73	74	3	2494 ± 30	3402 ± 406	0.75 ± 0.92
5	0.88	1.04	0.96	0.96	27	3	3118 ± 94	6144 ± 2341	10.7 ± 9.9
6	1.04	1.45	1.25	1.23	23	2	3804 ± 94	3359 ± 1072	3.1 ± 2.8

Table II: Properties of bins described in Sec. IIIB2 and values of the comoving distance \bar{D} , derivative of the comoving distance $D_{,z}$ and curvature parameter Ω_K measured in each bin. With z_{min} and z_{max} we indicate the left and right edge of each bin, respectively. z_i refers to the redshift at the centre of each bin, to which the mean distance \bar{D} has been assigned, while \bar{z} is the mean redshift of the bin.

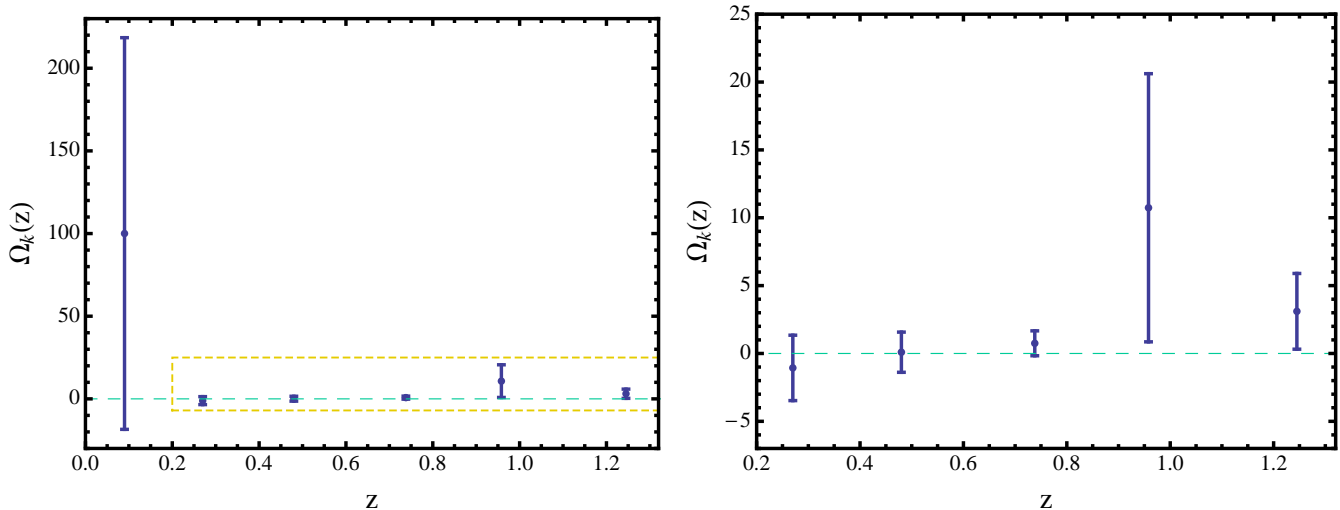


Figure 4: The curvature parameter Ω_K obtained by using $H(z)$ data from passively evolving galaxies and SnIa data and applying to them the binning procedure described in Sec. IIIB2. The dashed light-blue long-dashed line corresponds to the case of a flat FRW universe. On the left panel we show our full results, while on the right panel we focus on the region inside the yellow dashed box, i.e. on redshifts where constraints are best: $z > 0.2$. We omit to show horizontal error bars in order not to make the plot too crowded and confusing.

is obtained here for $z_i = 0.48$, while the best relative error, $\sigma_{\Omega_K}/|\Omega_K| = 0.9$, is obtained at $z_i = 1.25$.

In order to understand how much the low number of $H(z)$ data affects the size of the error bars, we sum to the measured $H(z)$ data a simulated set with properties similar to those of the original set. In particular, the simulated data are built in the same redshift interval, $0.09 < z < 1.75$, as a random distribution around a Gaussian centred on the best fit flat LCDM cosmology of the $H(z)$ data ($\Omega_m = 0.32$, $H_0 = 0.69$). The scatter around the Gaussian has been taken as the mean error of the real data points, while the error on the simulated data points has been simulated by taking a random distribution around a Gaussian with mean the mean error and variance the variance of the errors of the real data points. In order to reflect the different properties of the data distribution at low and high redshift, the redshift interval has been split into two equal parts, for which the simulated data have been produced separately. We then analyse the new resulting dataset and find that the errors on Ω_K remain comparable to those obtained from the smaller real dataset: differences are smaller than 17%. Even if we simulate a set 10 times larger than the present one, and if we reduce the scatter and error by a factor of 10, the difference in σ_{Ω_K} , for data at $z > 0.2$, is smaller than 64%. This means that, in order to obtain a noticeable improvement in the errors, not only the $H(z)$ data but also the SnIa dataset has to improve substantially.

Let us now compare the results of the two different binnings. If we look at the right panel of Fig. 3, we note that this second binning, corresponding to the red error bars, produces better results everywhere except around $z \sim 1$. After performing a number of tests, we found that this difference is mainly due to the large difference between the values of $D_{,z}$ in the two binnings (see bottom panel of Fig. 2), due in turn to the strong fluctuations of D around $z \sim 1$, that make results in proximity of $z = 1$ very binning-dependent.

Although this latter binning produces better results than the previous one, errors on Ω_K are still very large. In the

next section we will therefore describe and use a different technique to measure Ω_K .

C. Principal Component Analysis

In this section we will use the principal component analysis (PCA) to reconstruct the Hubble parameter and the comoving distance.

Following [47], the Hubble parameter and the luminosity distance can be modeled in terms of the deceleration parameter $q(z)$. The big advantage of this method, instead of considering the PCA for instance for $w(z)$ as it is common in the literature, is that the results for the deceleration parameter do not depend on Ω_m or any other parameter. Now, assuming that the deceleration parameter is constant in each bin, let us write it as

$$q(z) = \sum_{i=1}^n q_i \theta(z_i) \quad (14)$$

where the q_i are constant in each redshift bin z_i and $\theta(z_i)$ is the step-function, i.e. $\theta(z_i) = 1$ for $z_{i-1} \leq z \leq z_i$ and 0 elsewhere; then the Hubble parameter can be written (assuming that z is in the n -th bin) as

$$H_n(z) = H_0 c_n (1+z)^{1+q_n} \quad (15)$$

where the coefficient c_n is

$$c_n = \prod_{j=1}^{n-1} (1+z_j)^{q_j - q_{j+1}}. \quad (16)$$

Consequently, we can evaluate the luminosity distance by simply integrating Eq. (15) and we find:

$$d_{L,n}(z) = \frac{c}{H_0} (1+z) \left[f_n - \frac{(1+z)^{-q_n}}{c_n q_n} \right] \quad (17)$$

where

$$f_n = \frac{(1+z_{n-1})^{-q_n}}{c_n q_n} + \sum_{j=1}^{n-1} \frac{(1+z_{j-1})^{-q_j} - (1+z_j)^{-q_j}}{c_j q_j} \quad (18)$$

and $z_0 = 0$. Some more details regarding the derivation of the previous equations are shown in Appendix A. Also, it should be stressed that in all the calculations related to the PCA, the redshifts z_i correspond to the right edge of the bins and are not the average redshifts of the bins, see also Appendix A.

We decided to express the above quantities in term of the deceleration parameter $q(z)$; however the reader might think that a natural choice would be to choose a stepwise Hubble parameter. The reason why we choose to parameterize our quantities in terms of $q(z)$ is because the deceleration parameter varies slower at high redshift than, for instance, the Hubble parameter.

Next, we want to find the best fit parameters q_n by using two different data sets: Hubble measurements and luminosity distance measurements from SnIa. However, the two redshift ranges are different: while the measurements of SnIa reach $z \simeq 1.41$, those of the Hubble parameter reach $z = 1.80$. For our purpose, we assume constant q for each redshift bin and we divide the survey into 6 redshift bins up to $z = 1.45$; in particular, the binning is the same as that of Sec III B 2: $\{0, 0.18, 0.36, 0.6, 0.876, 1.04, 1.45\}$ (see previous subsection for details). To determine the best fit parameters q_n , we use a Monte Carlo Markov Chain (MCMC) method [48]; the best fits for both data sets are shown in Tab. III

Now in order to use the PCA to decorrelate the parameters q 's, we follow Ref. [49]. We first build a diagonal matrix Λ_{ij} with the eigenvalues of the Fisher matrix F_{ij} , which is defined as the inverse of the covariance matrix C_{ij} (obtained directly from the chains). Then we define a matrix $\tilde{W}_{ij} = W_{ik}^T \Lambda_{km}^{1/2} W_{mj}$ where the matrix W_{km}^T is the transpose of W_{km} and the latter is a matrix composed by the eigenvectors of Fisher matrix. We finally normalize \tilde{W}_{ij} such that its rows sum up to unity. The matrix \tilde{W}_{ij} will give the uncorrelated parameters, i.e. $p_i = \sum_{j=1}^M \tilde{W}_{ij} q_j$, where M is the total number of parameters. The variance of the parameters p_i will then be $\sigma^2(p_i) = 1/\lambda_i$. In Fig. 5 we show the deceleration parameter q for both $H(z)$ and SnIa measures for our 6 bins.

Parameters	$H(z)$		SnIa	
	q 's	1σ	q 's	1σ
q_1	-0.235357	2.1714	-0.516911	0.135228
q_2	0.125349	0.997989	-0.477117	0.342401
q_3	-0.574964	1.06027	0.290415	0.565752
q_4	-0.0301597	0.966473	-0.716238	1.02752
q_5	3.03175	1.8193	1.95358	3.01709
q_6	-0.301256	0.905626	-1.94705	2.02836

Table III: Best fit of the q_n parameters from the MCMC simulation and their corresponding 1σ errors for both Hubble and SNIa measurements.

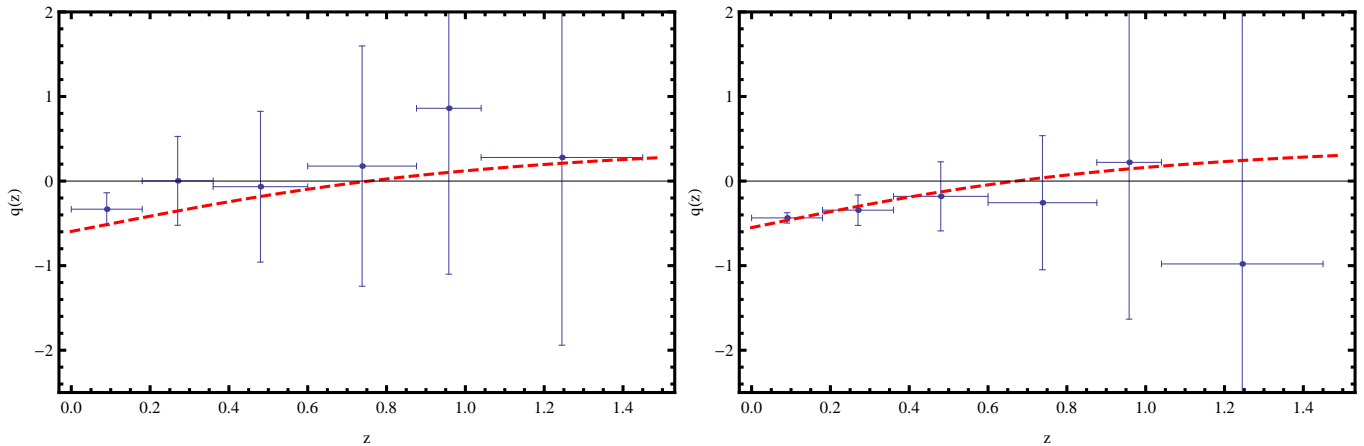


Figure 5: We show the deceleration parameter for the two data sets, $H(z)$ (left panel) and SnIa (right panel), using the PCA technique. As an example, we also report the deceleration parameter of the Λ CDM model (red dashed line).

Finally, we are in the position to evaluate the values of Ω_K for the six different bins. We want to remind the reader that we are using two different data sets to evaluate the q 's parameters: one for $H(z)$ and the other one for $D(z)$. In practice, to evaluate the Hubble parameter we will make use of the best fit of q obtained using the $H(z)$ data, whereas to evaluate the comoving distance $D(z)$ we will use the best fit of q obtained using the SnIa data. The curvature parameter will then be

$$\Omega_K(z, q_n) = \frac{[H_n(z; q_{n,H})D(z; q_{n,SN})]^2 - 1}{[H_0 D(z; q_{n,SN})]^2} \quad (19)$$

Parameters	$H(z)$		SnIa	
	q 's	1σ	q 's	1σ
q_1	-0.33247	0.19404	-0.435408	0.0609644
q_2	0.00281	0.52534	-0.343985	0.179551
q_3	-0.06639	0.89137	-0.180596	0.408267
q_4	0.17728	1.42054	-0.256041	0.792702
q_5	0.86084	1.96141	0.221318	1.85372
q_6	0.27898	2.21949	-0.979667	3.23438

Table IV: Principal component values from the MCMC analysis and their corresponding 1σ errors for both Hubble and SNIa measurements.

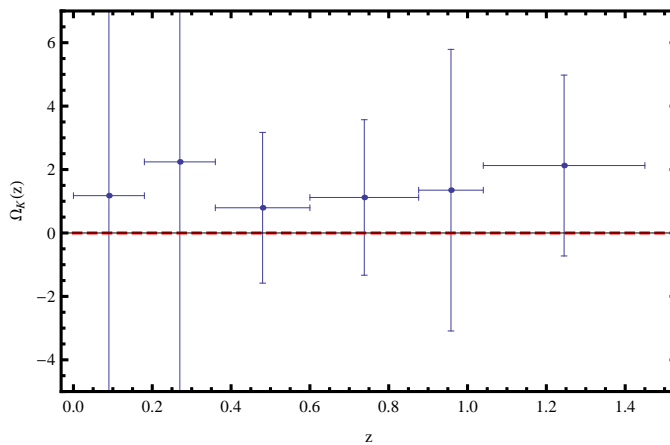


Figure 6: We show the curvature parameter computed by combining the two data sets, $H(z)$ and SnIa, using the PCA technique. The red dashed line refers to the flat FLRW model.

Parameters	Ω_K 's	1σ
Ω_{K_1}	1.17677	25.2965
Ω_{K_2}	2.24179	7.5252
Ω_{K_3}	0.794552	2.3758
Ω_{K_4}	1.11986	2.4511
Ω_{K_5}	1.34971	4.4396
Ω_{K_6}	2.12658	2.8511

Table V: Values of the curvature parameters at different redshifts and their corresponding 1σ errors using the PC analysis.

and the errors on Ω_K have been evaluated by using

$$\sigma_{\Omega_K}^2 = \sum_{i,j} \frac{\partial \Omega_{k,q_n}}{\partial q_i} C_{ij} \frac{\partial \Omega_{k,q_n}}{\partial q_j} \Big|_H + \sum_{k,l} \frac{\partial \Omega_{k,q_n}}{\partial q_k} C_{kl} \frac{\partial \Omega_{k,q_n}}{\partial q_l} \Big|_{SN} \quad (20)$$

where C_{ij} and C_{kl} are the covariance matrices of the q parameters using Hubble data and SnIa data, respectively.

In Fig. 6 we show the errors on the Ω_k for our 6 bins and in Tab. V we report their values. Clearly, the currently available data are not able to constrain the curvature parameter with sufficient accuracy and little can be said about Ω_K as the relative errors are of the order of few 100%.

The binning technique, showed in the previous section, and the PCA are somehow equivalent: we decide to divide the survey in different bins and we evaluate all the quantities in each bin. However, as previously stated, the principal component analysis gives substantially better results because we are decorrelating the parameters in each bin. In practice, we use a transformation matrix that is composed by the eigenvectors of the correlation matrix. The eigenvectors form an orthogonal basis to which the old set of parameters are projected to, hence the new parameters (which are a linear combination of the old set of parameters) will be uncorrelated; as a consequence the errors on the new set of parameters will be in general smaller than the errors of the *untransformed* parameters.

D. Genetic Algorithms

In what follows we will briefly describe the Genetic algorithms (GA). For more details and cosmological applications of GA see [50–52]. The GAs are based on the principles of evolution through natural selection, where a group of individuals, the “population”, evolves over time under the joined influence of two operators: the crossover (the combination of two or more different individuals) and the mutation (a random change in an individual). The probability of the “reproductive success” that an individual will produce offspring is directly proportional to the fitness of the individual. In our case the fitness is taken to be the χ^2 function, and it measures how accurately each individual describes the data.

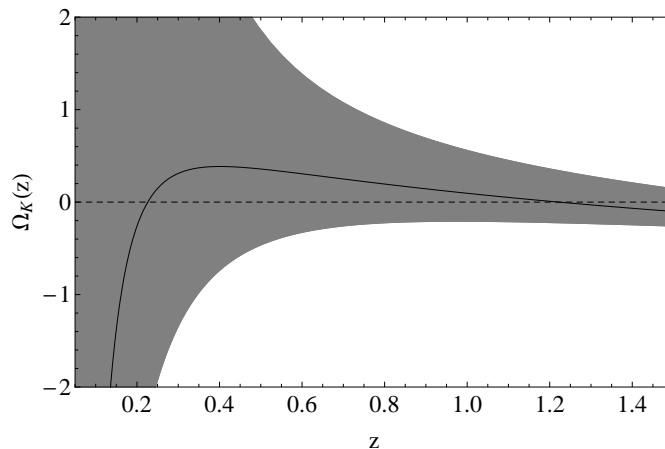


Figure 7: The reconstruction of $\Omega_K(z)$ from the GA. In both cases the gray region is the 1σ error and the solid line the best-fit. Clearly, it is consistent with $\Omega_K = 0$.

The algorithm starts with a group of individuals, the population, which in our case are sets of functions randomly generated based on a predetermined set of functions, the grammar, e.g. exp, sin, log etc, and a chosen set of operations, e.g. +, -, \times , \div . In each generation, the fitness for each individual of the population is evaluated and the operations of crossover and mutation are applied. This process is repeated several thousand times until certain termination criteria are reached, e.g. the maximum number of generations or the desired degree of convergence has been achieved. Then the best-fit solution can be used to extract the cosmological parameters or other quantities of interest.

In Fig. 7 we show the results of the application of the GA on the data and the reconstruction of Ω_K of Eq. (6) from the $H(z)$ and SnIa data. In this case, we used the $H(z)$ data to get $H(z)$ directly, while $D(z)$ was obtained from the SnIa. The error regions (gray bands) were made with the path integral formalism of [52] and correspond to the 1σ error. From Fig. 7 it is clear that the reconstruction is consistent with $\Omega_K = 0$. The main advantage of using the GAs in this case is that we can obtain model-independent constraints of the parameters of interest and, as we will see in later sections, they are in excellent agreement especially with the Padé approximation. The reason for the increased errors at small redshift will be explained in the last Section. Overall, we find that the GAs give the smallest error on Ω_K , $\sigma_{\Omega_K} \sim 0.1$, due to the fact that the method itself provides a smooth and analytical expression at all redshifts, compared to the binning methods. Also, it is somewhat better than the Padé method due to its better flexibility and non-parametric approach when fitting the data.

E. Padé approximation

In this section we followed a different approach in reconstructing the Hubble parameter, called *Padé approximation*. The main advantage in following this approach is that it gives the best approximation of a function by using only rational functions. Following [47] (and references therein), the Hubble parameter and the luminosity distance can be modeled by only two parameters, (a, b) . The $H(z)$ and $D(z)$ are

$$H(z) = H_0 \left[\frac{1 + b(1+z)^3}{1+b} \right]^{\frac{a+b}{3b}} \quad (21)$$

and

$$H_0 d_L(z) = (1+z)(1+b)^{\frac{a+b}{3b}} \left\{ (1+z) {}_2F_1 \left[\frac{a+b}{3b}, \frac{1}{3}, \frac{4}{3}; -b(1+z)^3 \right] - {}_2F_1 \left[\frac{a+b}{3b}, \frac{1}{3}, \frac{4}{3}; -b \right] \right\}, \quad (22)$$

where ${}_2F_1$ is the Gauss hypergeometric function. It is interesting to notice that we can recover the Λ CDM model by just setting $(a, b) = (\Omega_{m_0}/2\Omega_{\Lambda_0}, \Omega_{m_0}/\Omega_{\Lambda_0})$ into Eq. (21).

Using the $H(z)$ data and SnIa data we can calculate two independent sets of parameters (a, b) (best fit) and their corresponding errors simply by a likelihood analysis.

- **Hubble data:**

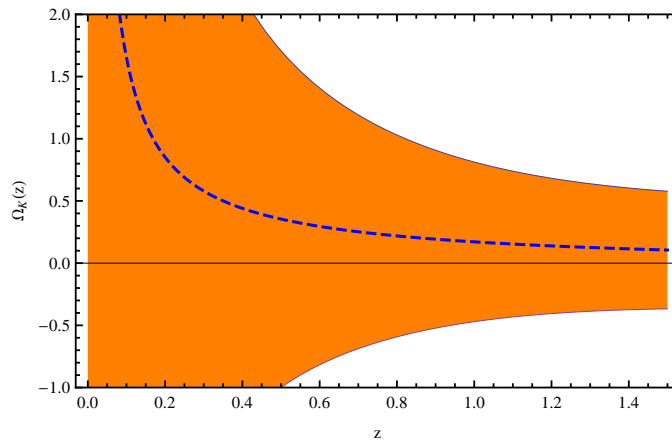


Figure 8: We plot the Ω_K as a function of redshift (blue dashed line) and the superposed error region (orange region).

Our χ^2 is defined as usual as

$$\chi^2 = \sum_{i=1}^n \frac{[H_i - H(a, b, z_i)]^2}{\sigma_i^2} \quad (23)$$

where H_i and σ_i are the Hubble data and their errors, respectively, and $H(a, b, z_i)$ is given by Eq. (21). We marginalize over H_0 .

The best fit and the corresponding 1σ errors are: $(a_H, b_H) = (0.23 \pm 0.07, 0.53 \pm 0.72)$

• SnIa data

In this case, the χ^2 is

$$\chi^2 = \sum_{i=1}^n \frac{[\mu_i - \mu(a, b, z_i)]^2}{\sigma_i^2} \quad (24)$$

where μ_i and σ_i are the SnIa distance moduli and their errors, respectively; the distance moduli $\mu(a, b, z_i)$ will be given by Eq. (9).

The best fit and the corresponding 1σ errors are: $(a_{SN}, b_{SN}) = (0.19 \pm 0.15, 0.39 \pm 0.46)$

Once the parameters a and b have been found for both datasets, we can reconstruct the Hubble parameter and comoving distance and hence the curvature parameter. In Fig. 8 we plot the curvature parameter as a function of redshift and the corresponding error region. The errors have been evaluated using Eq. (20) where q_i are now simply the two parameters a and b . We find that the constraints that we can give on the curvature parameter are very weak as the noise is much larger than the constraint itself.

IV. FORECASTS FROM THE EUCLID SURVEY

In this section we will now study the sensitivity with which the Euclid experiment³ [40, 41] will be able to constrain the curvature parameter Ω_K at different redshifts.

Euclid [41] is a medium-size mission of the ESA Cosmic Vision programme whose launch is planned for 2020. It will perform two surveys: a photometric survey in the visible and in three near-infrared bands, to measure weak gravitational lensing maps by imaging ~ 1.5 billion galaxies, and a spectroscopic slitless survey of ~ 50 million galaxies. Both surveys will be able to constrain both the expansion and the growth history of the Universe and will cover a total area of 15,000 square deg.

³ <http://www.euclid-ec.org/>

Our fiducial Euclid survey follows the specifications which can be found in the Euclid Definition Study Report (also called Red Book) [41]. As a fiducial model for our Fisher analysis we choose the WMAP-7 flat Λ CDM cosmology, as also used in the Euclid Red Book [41]. This means that we have $\Omega_{m_0} h^2 = 0.13$, $\Omega_{b,0} h^2 = 0.0226$, $\Omega_\Lambda = 1 - \Omega_{m_0} = 0.73$, $H_0 = 71$, $n_s = 0.96$ (where n_s is the scalar spectral index) and $w = -0.95$. The matter power spectrum was computed using CAMB⁴ [53]. More specifically, in this paper we only exploit the BAOs in the galaxy power spectrum as a standard ruler, in order to constrain the angular diameter distance and consequently the curvature parameter.

A. The angular diameter distance

Let us consider again the expression for the curvature parameter:

$$\Omega_K(z) = \frac{[H(z) D_{,z}(z)]^2 - 1}{[H_0 D(z)]^2}. \quad (25)$$

Our aim in this section is to put constraints on the curvature parameter in different redshift bins starting from BAO data. To this end we need an expression for the angular diameter distance. We can invert Eq. (25) and we have:

$$\frac{\partial D(z)}{\partial z} = \pm \frac{1}{H(z)} \sqrt{1 + H_0^2 D^2(z) \Omega_K(z)}. \quad (26)$$

We obtained an expression for the comoving distance which depends on the curvature density parameter. In order to use the expression above in our Fisher matrix calculation, we just use the finite approximation of the derivative of a function. Let us rewrite Eq. (26) in the following form:

$$\frac{\partial D(z)}{\partial z} \simeq \frac{D(z_{n+1}) - D(z_n)}{\Delta z_n} = \pm \frac{1}{H(z)} \sqrt{1 + H_0^2 D^2(z_n) \Omega_K(z_n)} \quad (27)$$

where Δz_n corresponds to the width of the bins (assumed to be constant). From Eq. (27) we can derive the expression for $D(z)$ valid for each bin:

$$D_{n+1} = D_n + \frac{\Delta z_n}{H_n} \sqrt{1 + \Omega_{K_n} H_0^2 (1 + z_n)^2 D_n^2}. \quad (28)$$

Since for the BAO Fisher matrix analysis we need the angular diameter distance D_A , we rewrite Eq. (28) as:

$$D_A(n+1) = \frac{1 + z_n}{1 + z_{n+1}} D_A(n) + \frac{1}{1 + z_{n+1}} \frac{\Delta z_n}{H_n} \sqrt{1 + \Omega_{K_n} H_0^2 (1 + z_n)^2 D_A^2(n)}. \quad (29)$$

where $D_A(n)$ refers to the angular diameter distance evaluated in the n -th bin.

The derivatives of $D_A(n+1)$ with respect to the Ω_{K_j} (curvature parameter in the j -th bin) are:

$$\begin{aligned} \frac{\partial D_A(n+1)}{\partial \Omega_{K_j}} &= \frac{1 + z_n}{1 + z_{n+1}} \frac{\partial D_A(n)}{\partial \Omega_{K_j}} + \frac{\Delta z_n}{2 H_n (1 + z_{n+1})} \frac{H_0^2 (1 + z_n)^2 D_A^2(n)}{\sqrt{1 + \Omega_{K_n} H_0^2 D_A^2(n)}} \frac{\partial \Omega_{K_n}}{\partial \Omega_{K_j}} + \\ &+ \frac{\Delta z_n}{H_n (1 + z_{n+1})} \frac{H_0^2 (1 + z_n)^2 D_A(n) \Omega_{K_n}}{\sqrt{1 + \Omega_{K_n} H_0^2 (1 + z_n)^2 D_A^2(n)}} \frac{\partial D_n}{\partial \Omega_{K_j}}. \end{aligned} \quad (30)$$

We choose now to take into account the derivative of the H_n with respect to the curvature parameter Ω_{K_j} . This is because we are assuming that the measurements of the Hubble parameters should be independent of those of D_A (we will come back to this in the next section). For the Fisher matrix analysis we need to evaluate the derivatives for a reference cosmology. Our reference cosmology is flat Λ CDM, hence $\Omega_{K_i} = 0$. For this fiducial model, Eq. (30) can be written as:

$$\frac{\partial D_A(n+1)}{\partial \Omega_{K_j}} = \frac{1 + z_n}{1 + z_{n+1}} \left. \frac{\partial D_n}{\partial \Omega_{K_j}} \right|_{\Omega_{K_j}=0} + \frac{1}{2 H_n} \frac{\Delta z_n}{1 + z_{n+1}} H_0^2 (1 + z_n)^2 D_A^2(n) \left. \delta_{K_j K_n} \right|_{\Omega_{K_j}=0}. \quad (31)$$

⁴ <http://camb.info>

The second term of the above equation contains a delta of Kronecker, $\delta_{K_j K_n}$, that is non zero only if $\Omega_{K_j} = \Omega_{K_n}$. The first term on the right hand side of Eq. (31) exists only if $j < n$, and this can be easily seen from Eq. (28), where the comoving distance in one bin depends on Ω_k of the previous bin. Let us now assume that $j < n$; then Eq. (31) becomes:

$$\frac{\partial D_{n+1}}{\partial \Omega_{K_j}} = \frac{1+z_n}{1+z_{n+1}} \frac{\partial D_n}{\partial \Omega_{K_j}} \Big|_{\Omega_{K_j}=0}. \quad (32)$$

This can be further simplified just by realizing that if we take the derivative of D_n with respect to Ω_{K_j} we are still left with a term containing the delta of Kronecker, which is non zero only if $j = n-1$, and another term containing the derivative of D_{n-1} , which is non zero only if $j < n-1$. Proceeding by iteration we are left with:

$$\begin{aligned} \frac{\partial D_A(n+1)}{\partial \Omega_{K_j}} &= \frac{1+z_n}{1+z_{n+1}} \frac{\partial D_A(n)}{\partial \Omega_{K_j}} = \frac{1+z_n}{1+z_{n+1}} \frac{1+z_{n-1}}{1+z_n} \frac{\partial D_A(n-1)}{\partial \Omega_{K_j}} = \frac{1+z_{n-1}}{1+z_{n+1}} \frac{1+z_{n-2}}{1+z_{n-1}} \frac{\partial D_A(n-2)}{\partial \Omega_{K_j}} = \\ &= \dots = \frac{1+z_{j+2}}{1+z_{n+1}} \frac{1+z_{j+1}}{1+z_{j+2}} \frac{\partial D_A(j+1)}{\partial \Omega_{K_j}} \end{aligned} \quad (33)$$

hence, Eq. (33) becomes:

$$\frac{\partial D_A(n+1)}{\partial \Omega_{K_j}} = \frac{1+z_{j+1}}{1+z_{n+1}} \frac{\partial D_A(j+1)}{\partial \Omega_{K_j}}. \quad (34)$$

Let us now assume that $j = n$; then Eq. (31) reads:

$$\frac{\partial D_A(j+1)}{\partial \Omega_{K_j}} = \frac{(1+z_j)^2}{2H_j} \frac{H_0^2 D_A^2(j) \Delta z_j}{1+z_{j+1}} \Big|_{\Omega_{K_j}=0}. \quad (35)$$

We remind the reader that Eqs. (33) and (35) are valid as long as all the Ω_{K_j} in the reference cosmology are zero (of course a more general formula could be found but this goes beyond the goal of this work). We have now two different derivatives for the angular diameter distance depending on the bin. By iteration, we can write Eq. (29), in the reference cosmology, as:

$$D_A(n+1) = \frac{1+z_1}{1+z_{n+1}} D_A(1) + \frac{1}{1+z_{n+1}} \sum_{k=1}^n \frac{\Delta z_n}{H_n}. \quad (36)$$

Then, Eqs. (33) and (35), together with Eq. (36), become:

$$\frac{\partial D_A(n+1)}{\partial \Omega_{K_j}} = \begin{cases} \frac{H_0^2}{2H_j} \frac{\Delta z_j}{1+z_{j+1}} \left[(1+z_1) D_A(1) + \sum_{k=1}^{j-1} \frac{\Delta z}{H_k} \right]^2 \Big|_{\Omega_{K_j}=0}, & \text{if } j = n \\ \frac{H_0^2}{2H_j} \frac{\Delta z_j}{1+z_{n+1}} \left[(1+z_1) D_A(1) + \sum_{k=1}^{j-1} \frac{\Delta z}{H_k} \right]^2 \Big|_{\Omega_{K_j}=0}, & \text{if } j < n \end{cases} \quad (37)$$

The derivatives of the logarithm of the angular diameter distance with respect to the curvature parameter, needed for the computation of the BAO Fisher matrix are finally:

$$\frac{\partial \ln D_A(n+1)}{\partial \Omega_{K_j}} = \begin{cases} \frac{H_0^2}{2H_j} \Delta z_j \frac{[(1+z_1)D_A(1) + \sum_{k=1}^{j-1} \frac{\Delta z}{H_k}]^2}{(1+z_1)D_A(1) + \sum_{k=1}^j \frac{\Delta z}{H_k}} \Big|_{\Omega_{K_j}=0}, & \text{if } j = n \\ \frac{H_0^2}{2H_j} \Delta z_j \frac{[(1+z_1)D_A(1) + \sum_{k=1}^{j-1} \frac{\Delta z}{H_k}]^2}{(1+z_1)D_A(1) + \sum_{k=1}^n \frac{\Delta z}{H_k}} \Big|_{\Omega_{K_j}=0}, & \text{if } j < n \end{cases} \quad (38)$$

B. Fisher matrix formalism

Let us now show and comment on the Fisher matrix forecasts for the Euclid galaxy *redshift* survey. Following [54], we write the observed galaxy power spectrum as:

$$\begin{aligned} P_{obs}(z, k_r) &= \frac{D_{Ar}^2(z)H(z)}{D_A^2(z)H_r(z)} G^2(z)b(z)^2 (1+\beta\mu^2)^2 P_{0r}(k) \\ &+ P_{shot}(z) \end{aligned} \quad (39)$$

Parameters		
1	Reduced Hubble	h
2	Total matter density	$\omega_m = \Omega_{m_0} h^2$
3	Total baryon density	$\omega_b = \Omega_{b_0} h^2$
4	Spectral index	n_s
5	Growth index	γ
	<i>For each redshift bin</i>	
6	Shot noise	P_s
7	Redshift space distortion	$\log \beta$
8	Growth Factor	$\log G$
9	Angular diameter distance	$\log D_A$
10	Hubble	$\log H$

Table VI: Cosmological parameters for the Fisher matrix analysis

where the subscript r refers to the values assumed for the reference cosmological model, i.e. the model at which we will evaluate the Fisher matrix. Here P_{shot} is the shot noise due to discreteness in the survey, μ is the cosine of the angle of the wave mode with respect to the line of sight, $P_{0r}(k)$ is the present matter power spectrum for the fiducial cosmology, $G(z)$ is the linear growth factor of matter perturbations, $b(z)$ is the bias factor. The wavenumber k has also to be written in terms of the fiducial cosmology ([54] and see also [55] and [56] for more details).

The spectroscopic survey covers a redshift range of $0.65 < z < 2.05$, which we divide into 14 bins of equal width $\Delta z = 0.1$. Regarding the bias, we assume it to be scale-independent, since this is a quite good approximation for the large linear scales which we will use. Our fiducial bias was derived by [57] using a semi-analytical model of galaxy formation, and it is the same bias function used for the Euclid Red Book forecasts. The expected galaxy number densities which we used can be found in [58] and were computed by using a sophisticated simulation [59]. The maximum scale R used are such that $\sigma^2(R) \leq 0.25$, with an additional cut at $k_{\max} = 0.20 h \text{ Mpc}^{-1}$ to avoid non-linearity problems. The wavenumber k is also to be transformed between the fiducial cosmology and the general one.

The parameters that we use for evaluating the Fisher matrix are shown in Tab. VI. We evaluated the linear matter power spectrum P_{0r} using CAMB, see [53]. Once we have the full Fisher matrix, we marginalize over all the parameters but the angular diameter distances. We obtain a submatrix with only D_A, \mathcal{F}_{mn} . The new Fisher matrix for the Ω_K will be given by:

$$F_{\Omega_{K_i} \Omega_{K_j}} = \frac{\partial \log D_A(m)}{\partial \Omega_{K_i}} \mathcal{F}_{mn} \frac{\partial \log D_A(n)}{\partial \Omega_{K_j}} \quad (40)$$

where the derivatives $\frac{\partial \log D_A(n)}{\partial \Omega_{K_j}}$ are given by Eq. (38). In this work we are using only the information coming from the measurements of the angular diameter distance and we are ignoring the information of the Hubble parameter (by simply neglecting the derivative of Hubble parameter with respect to the Ω_K 's). This is because the Fisher matrix analysis has been done assuming a reference cosmology, i.e. flat Λ CDM; with this assumption, the Hubble parameter and the angular diameter distance are not independent quantities, so taking into account in our analysis the two parameters would bias our results. Choosing to neglect the derivatives of the Hubble parameter with respect to Ω_K means that we assume $H(z)$ to be measured with infinite precision by another experiment. Anticipating the results, our analysis shows that even with this strong, and very optimistic, assumption the sensitivity of the Euclid satellite in constraining the curvature parameter is not enough to rule out inhomogenous models, like for instance the LTB model shown in Fig. (10). In [24], the authors also forecasted the measurement of the curvature parameter with the Euclid survey, using a different fiducial cosmology. In their analysis they consider both the Hubble parameter and angular diameter distance; this is why the errors they found on the curvature parameter are of a factor 2 – 3 larger than our results.

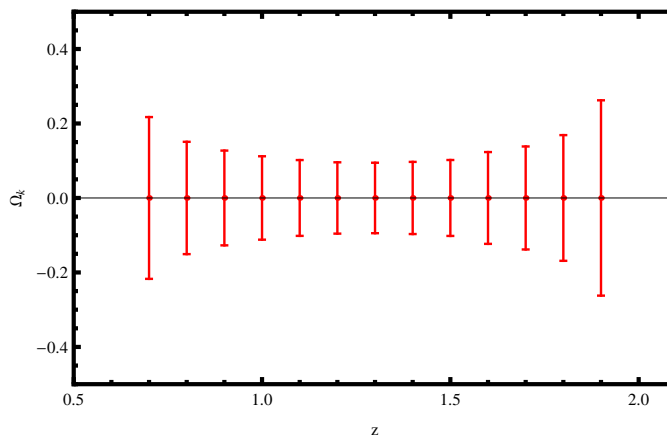


Figure 9: Error bars for the curvature parameter using the Euclid survey only.

	z	0.7	0.8	0.9	1.0	1.1	1.2	1.3	1.4	1.5	1.6	1.7	1.8	1.9
Euclid	$\sigma(\Omega_k)$	0.2172	0.1508	0.1272	0.1119	0.1017	0.0957	0.0946	0.0968	0.1019	0.1232	0.1382	0.1687	0.2621
Case 1	$\sigma(\Omega_k)$	0.1820	0.1336	0.1133	0.0998	0.0903	0.0843	0.0816	0.0811	0.0819	0.0881	0.0910	0.0932	0.0981
Case 2	$\sigma(\Omega_k)$	0.0962	0.0781	0.0671	0.0591	0.0530	0.0484	0.0450	0.0424	0.0401	0.0386	0.0369	0.0352	0.0338

Table VII: Errors for the curvature parameter using Euclid only, adding SnIa case 1) and case 2).

C. Adding the supernovae

To add the SnIa, we first compute the corresponding Fisher Matrix. We present the details of the cumbersome calculations in Appendix B. In this case, the most important quantity is the marginalized error on $\log D_i/D_1$, which is given by [60]

$$(F)_{ii}^{-1} = \frac{2\sigma^2}{a^2 N} \approx 0.42 \frac{\sigma^2}{N}. \quad (41)$$

D. Results

In Fig. 9 we show the errors on Ω_K for each redshift bin. As we can see, we lose the information on the last bin; this is due to the fact that the information on the curvature parameter in one bin depends on the angular diameter distance of the next bin. In Fig. 10 we show the errors on Ω_K for each redshift bin when adding to the Euclid forecasts the SnIa for two cases, i.e. for a number of SnIa $N = 100$ and for $N = 1000$. In Tab. VII we report the errors for each bin for Euclid only and for Euclid with the addition of the SnIa.

We notice that using Euclid data alone, the redshift region where errors are smallest is $1.1 < z < 1.5$. At lower and at higher redshifts constraints become worse by up to a factor of two and a half. Adding the first set of $N = 100$ SnIa does not change results substantially at low redshift, while it does improve constraints at redshifts $z > 1.5$. The second set of SnIa with $N = 1000$ instead improves constraints at all redshifts by a factor of ~ 2 and it moves the best constrained area to $z > 1.5$. In this case, one will have to worry about modeling the SnIa systematic errors, but this goes beyond the scope of our paper and is left to future work.

For comparison, we also plotted in the right panel of Fig. 10 the curve representing the behavior of the curvature parameter for the timescape scenario of [16], for the Tardis cosmology of [23], and for the LTB model given by [61]. The Euclid survey will not be able to rule out the latter class of models, not even when adding SnIa constraints, as these models are asymptotically flat homogeneous models. Only surveys that observe galaxies at low redshifts, with $z < 0.5$, will be able to rule out (or confirm) these models since they all manifest, at these redshifts, a very different

⁴ courtesy of David Wiltshire.

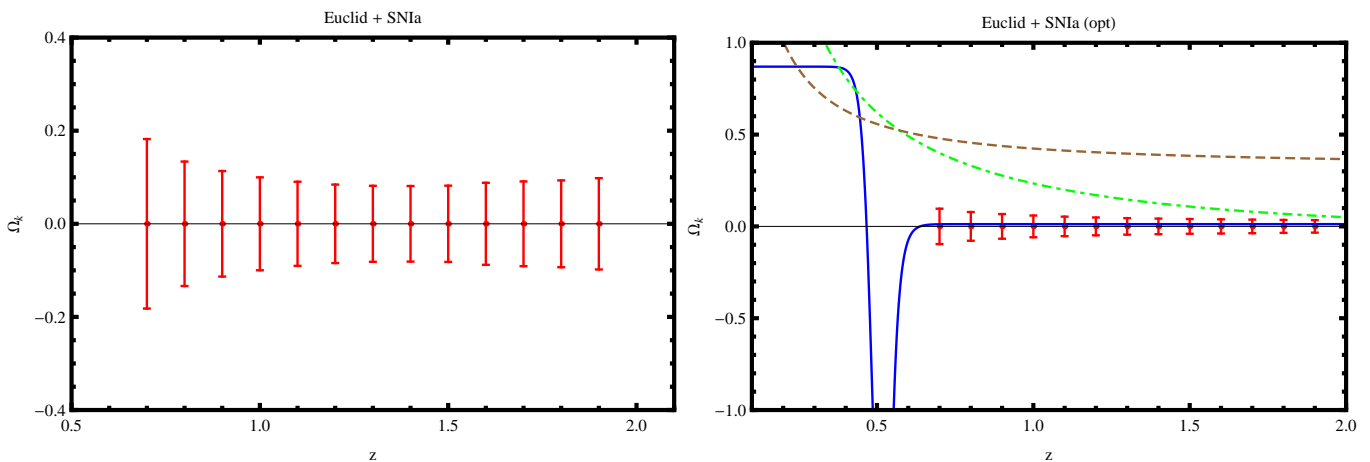


Figure 10: Error bars for the curvature parameter using Euclid and adding SnIa with: $N = 100$ and $N=1000$, left and right respectively. In the right panel we also plotted, as an example, three non-FLRW models. The blue solid line corresponds to the curvature parameter in the LTB model. The brown dashed line indicates the Tardis model as in Fig. 12 a) of [23] and is courtesy of Mikko Lavinto and Syksy Räsänen. The green dot-dashed line corresponds to the timescape scenario, see [16, 62] and is courtesy of David Wiltshire.

behavior from the flat FLRW model, as can be seen from Fig. 10. However, if a model has a value of Ω_K of about ~ 0.4 , we may be able to distinguish it from flat FLRW with Euclid future data.

V. CONCLUSIONS

In this paper we used four different methods to reconstruct, in a model-independent fashion, the Hubble parameter and the luminosity distance, measured by two different data sets. We find that all four methods used, i.e. direct binning, principal component, genetic algorithms and Padé approximation, give results that are in agreement with respect to their general behavior.

In particular, all four methods lead to very large errors at low redshifts, while errors decrease noticeably for larger z . The transition redshift is in all cases between 0.2 and 0.4. To be specific, as for the direct binning and the PCA techniques, the best measured Ω_K have errors $\sigma_{\Omega_K} \simeq 3$. For the genetic algorithms and Padé approximations instead, we found that the errors on the curvature parameter are of the order of about $\sigma_{\Omega_K} \sim 20$ at small redshifts, and they decrease when z grows, reaching a value of about $\sigma_{\Omega_K} \sim 0.5$ for redshifts $z \geq 1$. This means that reconstruction techniques manage to reduce the error if compared to techniques where data need to be binned. The best method, leading to the smallest error on Ω_K , $\sigma_{\Omega_K} \simeq 0.1$, is the one based on GA.

We also find that the choice of the binning, as expected, influences the values of the errors, by affecting mostly the derivative of the comoving distance. This is simply due to the nature of the SnIa data: in regions where the values of the distance modulus have large fluctuations, there will be a strong dependence of the choice of binning on the value of the derivative.

Going back to the problem of the large size of the errors at low redshifts, this may appear strange because here we have a large number of data with small errors (in particular as regards SnIa data, see e.g. Fig. 1). If we have a closer look though, we find that the main reason for this feature lays on the expression of Ω_K itself, so let us explain this in detail. The curvature parameter was found to be

$$\Omega_K = \frac{[H(z)D_{,z}(z)]^2 - 1}{[H_0 D(z)]^2}. \quad (42)$$

This expression tells us that if the Universe is not homogeneous then the curvature parameter has to vary with redshift, i.e. Ω_K is not constant. From Eq. (5) we learn that the comoving distance is the integral of the Hubble parameter; however, Eq. (5) has been evaluated under the assumption of homogeneity, as a consequence Ω_K can only be constant.

Now let us assume that, via one observable, we measure the Hubble parameter $H(z)$ and, via another independent observable, we measure the luminosity distance, which gives a slightly different Hubble parameter, say $H_1(z)$. Then,

substituting $H_1(z)$ in Eq. (5), Eq. (42) will look like:

$$\tilde{\Omega}_K(z) = \Omega_K \frac{1 - \left(\frac{H(z)}{H_1(z)}\right)^2 \cos^2 \left[\sqrt{-\Omega_K} \int_0^z \frac{H_0 dx}{H_1(x)} \right]}{\sin^2 \left[\sqrt{-\Omega_K} \int_0^z \frac{H_0 dx}{H_1(x)} \right]}, \quad (43)$$

where $\tilde{\Omega}_K$ is the function that we want to evaluate, whereas Ω_K is the standard curvature parameter. As we can see, for small redshifts, the numerator of Eq. (43) stays finite ($\cos(0) = 1$), but the denominator does not ($\sin(0) = 0$). Let us assume that for $z \rightarrow 0$, the quantity $\sqrt{\Omega_K} \int_0^z H_0 dx / H_1(x) \rightarrow \epsilon$, where ϵ is a small number that goes to zero when $z = 0$. Then, Eq. (43) reads

$$\tilde{\Omega}_K(z) = \Omega_K \frac{1 - \left(\frac{H(z)}{H_1(z)}\right)^2 \cos^2(\epsilon)}{\sin^2(\epsilon)} = \Omega_K \frac{1 - \left(\frac{H(z)}{H_1(z)}\right)^2 + \left(\frac{H(z)}{H_1(z)}\right)^2 \sin^2(\epsilon)}{\sin^2(\epsilon)} \quad (44)$$

For $\epsilon \rightarrow 0$, Eq. (44) becomes

$$\tilde{\Omega}_K(z) = \lim_{\epsilon \rightarrow 0} \left(\Omega_K \frac{1 - \left(\frac{H(z)}{H_1(z)}\right)^2 + \left(\frac{H(z)}{H_1(z)}\right)^2 \sin^2(\epsilon)}{\sin^2(\epsilon)} \right) \rightarrow \infty, \quad (45)$$

Then, in order for the above equation to stay finite at small redshift we need $H_1(z)$ to be exactly equal to $H(z)$; in other words, the curvature parameter stays constant at small redshifts if the Universe is homogeneous! This is the reason why for small redshifts, when measuring $H(z)$ and $D(z)$ with independent observations, the values of the curvature parameter (and their errors) are very large. In this paper, we used two different datasets which give, of course, two different best fits of the parameters and consequently these two best fits will give two different Hubble parameters ($H(z)$ and $H_1(z)$), so that Eq. (44) still diverges when $z \rightarrow 0$.

Alternatively, we can also perform a series expansion on Eq. (42) for small z . Doing so we find

$$\tilde{\Omega}_K = \Omega_k + \frac{1 - \frac{H_{1,0}^2}{H_0^2}}{z^2} + \frac{2H_0 H'(0) - H_{1,0} H_1'(0)}{H_0^2} - \frac{H_1'(0)}{H_{1,0}} + \dots, \quad (46)$$

where the primes denote a derivative with respect to z , eg $H_1'(0) = \frac{dH_1}{dz}|_{z=0}$, while H_0 and $H_{1,0}$ are the values of the two Hubble parameters at $z = 0$. The advantage of this approach is that we can also clearly see, in a model-independent way and without assuming a Dark Energy model, the type of the singularity as $z \rightarrow 0$. So, unless $H(z) = H_1(z)$ then there will be a singularity $\sim 1/z^2$ at $z = 0$.

To also prove numerically what is explained above, we report the case of the PCA analysis. Here the value of the Hubble parameter in each of the 6 bins, obtained when using the best fits from SnIa are: $H(z_i) = \{71.1431, 76.9306, 87.9404, 103.691, 108.447, 129.132\}$. When using the best fits from $H(z)$ measurements from passively evolving galaxies, we obtain instead: $H(z_i) = \{71.1061, 82.0685, 91.8856, 102.916, 131.697, 166.138\}$. The difference of the Hubble parameters in the first redshift bin is 0.037; even though this number is very small, it is not small enough to guarantee the curvature parameter to be stable at low redshifts.

The same conclusion was previously found by [23]⁵. Also [19] explain this feature of the Ω_K test, but their analysis was done assuming a particular dark energy model and the results could be different for different models. Here we have demonstrated that Eq. (42) always diverges at small redshifts independently of the model as $\sim 1/z^2$, for all models different from the homogeneous and isotropic one.

As a last remark, it is important to notice that in general the data are not free of systematics (and they are unavoidable), so even if the universe is homogeneous and isotropic, we will always reconstruct two different Hubble parameters from two different datasets, which will lead to a divergent (or very large) Ω_K at low redshifts. Probably the test of Ω_K will give a results that it is still consistent with the FLRW universe within the errors. Also, one should consider that there will always be a “noise” in the measurement of Ω_K due to the presence of inhomogeneities, that generate fluctuations on the measured values of the pure FLRW cosmological parameters [63].

Future data from the Euclid satellite will improve considerably the errors on the curvature parameter with respect to present data; in particular we will have an improvement of about 10 times when using Euclid only, and even up to 40 times if we add future SnIa data to the Euclid survey data.

⁵ However, here a divergence $\propto z^{-1}$ was found

Acknowledgments

We thank Luca Amendola who participated in the beginning of this project and for useful and interesting discussions afterwards. We also thanks Licia Verde and Antonio Enea Romano for fruitful discussions. S. N. and D. S. acknowledge financial support from the Madrid Regional Government (CAM) under the program HEPHACOS S2009/ESP-1473-02, from MICINN under grant AYA2009-13936-C06-06 and Consolider-Ingenio 2010 PAU (CSD2007-00060), as well as from the European Union Marie Curie Initial Training Network UNILHC Grant No. PITN-GA-2009-237920. E. M. was supported by the Spanish MICINNs Juan de la Cierva programme (JCI-2010-08112), by CICYT through the project FPA-2012-31880, by the Madrid Regional Government (CAM) through the project HEPHACOS S2009/ESP-1473 under grant P-ESP-00346 and by the European Union FP7 ITN INVISIBLES (Marie Curie Actions, PITN-GA-2011- 289442). All authors also acknowledge the support of the Spanish MINECO's "Centro de Excelencia Severo Ochoa" Programme under Grant No. SEV-2012-0249.

Appendix A: The PCA

The expressions for the PCA in terms of the deceleration parameter were derived in Ref. [47], but here we will present some more details about their derivation. Let us write the deceleration parameter as

$$q(z) = \sum_{i=1}^n q_i \theta(z_i), \quad (\text{A1})$$

where q_i are constant in each redshift bin z_i and $\theta(z_i)$ is the theta-function, i.e. $\theta(z_i) = 1$ for $z_{i-1} \leq z \leq z_i$ and 0 elsewhere. The general expression for the deceleration parameter is

$$1 + q(z) = \frac{d \ln(H(z))}{d \ln(1+z)}, \quad (\text{A2})$$

and this can be rewritten as

$$\ln(H(z)/H_0) = \int_0^z \frac{1+q(x)}{1+x} dx, \quad (\text{A3})$$

or

$$H(z)/H_0 = e^{I(z)} \quad (\text{A4})$$

$$I(z) = \int_0^z \frac{1+q(x)}{1+x} dx. \quad (\text{A5})$$

For $z \in (z_{i-1}, z_i]$ and using the fact that q is constant in each bin, we can break the integral $I(z)$ in parts as

$$\begin{aligned} I(z) &= \int_0^{z_1} (\dots) + \int_{z_1}^{z_2} (\dots) + \dots + \int_{z_{i-1}}^z (\dots) \\ &= (1+q_1) \ln(1+x)|_0^{z_1} + (1+q_2) \ln(1+x)|_{z_1}^{z_2} + \dots + (1+q_i) \ln(1+x)|_{z_{i-1}}^z \\ &= (1+q_1) \ln(1+z_1) + (1+q_2) \ln\left(\frac{1+z_2}{1+z_1}\right) + \dots + (1+q_i) \ln\left(\frac{1+z}{1+z_{i-1}}\right). \end{aligned} \quad (\text{A6})$$

Grouping the constant terms, the Hubble parameter can then be written, for z in the n -th bin, as

$$H_n(z) = H_0 c_n (1+z)^{1+q_n} \quad (\text{A7})$$

where the coefficient c_n is

$$c_n = \prod_{j=1}^{n-1} (1+z_j)^{q_j - q_{j+1}}. \quad (\text{A8})$$

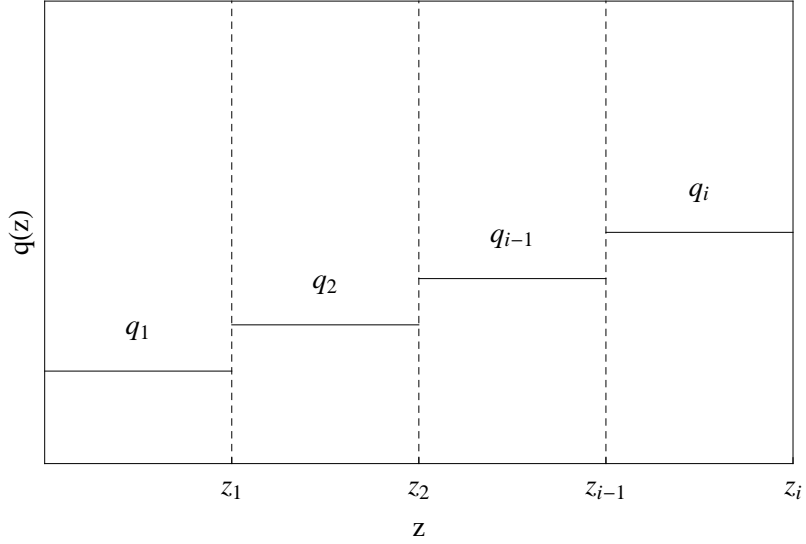


Figure 11: Example of a binning scheme. The derivations assume that the point of interest has $z \in (z_{i-1}, z_i]$, so that $q(z) = q_i$.

We can now follow a similar procedure to calculate the luminosity distance. Using the definition of the luminosity distance along with the previous equations we have

$$\begin{aligned}
 d_L(z) &= \frac{c}{H_0}(1+z) \int_0^z \frac{1}{H(z)/H_0} dz \\
 &= \frac{c}{H_0}(1+z) \left(\int_0^{z_1} (\dots) + \int_{z_1}^{z_2} (\dots) + \dots + \int_{z_{i-1}}^z (\dots) \right) \\
 &= \frac{c}{H_0}(1+z) \left(\frac{1 - (1+z_1)^{-q_1}}{c_1 q_1} + \frac{(1+z_1)^{-q_2} - (1+z_2)^{-q_2}}{c_2 q_2} + \dots + \frac{(1+z_{i-1})^{-q_i} - (1+z)^{-q_i}}{c_i q_i} \right). \quad (\text{A9})
 \end{aligned}$$

Collecting the constant terms, the latter can be written as

$$d_{L,n}(z) = \frac{c}{H_0} (1+z) \left[f_n - \frac{(1+z)^{-q_n}}{c_n q_n} \right], \quad (\text{A10})$$

where

$$f_n = \frac{(1+z_{n-1})^{-q_n}}{c_n q_n} + \sum_{j=1}^{n-1} \frac{(1+z_{j-1})^{-q_j} - (1+z_j)^{-q_j}}{c_j q_j}, \quad (\text{A11})$$

and $z_0 = 0$.

Appendix B: The SnIa Fisher Matrix

The SnIa likelihood is

$$\mathcal{L} = -2 \log L = \sum \frac{(m_i - m_{t,i} + M)^2}{\sigma_i^2} \quad (\text{B1})$$

where M is the overall offset (sum of the SnIa absolute magnitude, the Hubble constant and other things). We marginalize over M

$$L = \int \exp\left[-\frac{1}{2} \sum \frac{(m_i - m_{t,i} + M)^2}{\sigma_i^2}\right] dM = N e^{-\frac{1}{2} [S_2 - \frac{S_1^2}{S_0}]} \quad (\text{B2})$$

where

$$S_m = \sum \frac{(m_i - m_{t,i})^m}{\sigma_i^2} \quad (\text{B3})$$

To find the Fisher Matrix (FM) we calculate

$$F_{ij} = \frac{\partial(-\log L)}{\partial p_i \partial p_j} = \frac{1}{2} [S_{,ij}^2 - \frac{2}{S^0} (S_{,i}^1 S_{,j}^1 + S^1 S_{,ij}^1)] \quad (\text{B4})$$

where the cosmological parameters are the luminosity distances: $p_i = D_i$ inside each of the b bins. We have

$$m_{ti,j} = a \delta_{ij}, \quad a = 5/\log 10 \approx 2.17$$

where δ_{ij} is unity if the i -th SnIa belongs to the j -th bin, 0 otherwise. Then we have

$$S_{,i}^1 = -a S^{0B_i} \quad (\text{B5})$$

$$S_{,ij}^1 = 0 \quad (\text{B6})$$

$$S_{,ij}^2 = 2a^2 S^{0B_i} \delta_{ij} \quad (\text{B7})$$

where

$$S^{0B_i} = \sum_{B_i} \frac{1}{\sigma_i^2}$$

Then

$$F_{ij} = 2a^2 \left[S^{0B_i} \delta_{ij} - \frac{S^{0B_i} S^{0B_j}}{S^0} \right] \quad (\text{B8})$$

Suppose now that all errors are identical and equal to σ , so that $S^0 = n/\sigma^2$, $S^{0B_i} = N_{B_i}/\sigma^2$, $\sum N_{B_i} = n$. Then

$$F_{ij} = 2a^2 \frac{N_{B_i}}{\sigma^2} \left[\delta_{ij} - \frac{N_{B_j}}{n} \right] \quad (\text{B9})$$

This matrix is singular because

$$\sum_i \left(N_{B_i} \delta_{ij} - \frac{N_{B_i} N_{B_j}}{n} \right) = N_{B_j} - N_{B_j} = 0$$

We can however fix the first bin, i.e. assume that we know D_1 and then use as parameters $\log D_i/D_1$. The whole procedure remains the same because $\log D_1$ just adds to M and we just have to strip off the FM by the first row and column. We can put $N_{B_i} = N$ for simplicity, and having b bins, $bN = n$. Then we get

$$F = a^2 \frac{N}{\sigma^2} \left[I - \frac{1}{b} U \right] \quad (\text{B10})$$

where I is the identity matrix and U is formed by 1's everywhere. We can use this matrix to model the SnIa Fisher matrix. For instance if we have $b=3$ bins, with N SnIa each, then F is a 2x2 matrix for $\log D_2/D_1$ and $\log D_3/D_1$:

$$\frac{Na^2}{\sigma^2} \begin{pmatrix} 1 - \frac{1}{3} & -\frac{1}{3} \\ -\frac{1}{3} & 1 - \frac{1}{3} \end{pmatrix}$$

If needed, we must put zeros for rows and columns for unconstrained parameters (e.g. D_1, H_i). We assume two cases: 1) current data and 2) future data. For case 1) we put $\sigma = 0.3$ and $N = 100$, while for case 2) we assume the same σ but $N = 1000$.

The inverse of a matrix of rank r

$$M = \beta(I - \alpha U) \quad (\text{B11})$$

is

$$M^{-1} = \beta^{-1} \left(I - \frac{\alpha}{r\alpha - 1} U \right) \quad (\text{B12})$$

Our FM is of this form, with $r = b - 1$, $\alpha = 1/b$ and $\beta = a^2 N / \sigma^2$. Hence

$$F^{-1} = \frac{\sigma^2}{a^2 N} [I + U]. \quad (\text{B13})$$

The marginalized error on $\log D_i / D_1$ is finally

$$(F)_{ii}^{-1} = \frac{2\sigma^2}{a^2 N} \approx 0.42 \frac{\sigma^2}{N}. \quad (\text{B14})$$

-
- [1] A.G. Riess et al, *Astron. J.* **116**, 1009 (1998).
[2] D.N. Spergel et al., *ApJS* **148**, 175 (2003).
[3] M. Tegmark et al., *Phys. Rev. D* **69**, 103501 (2004); M. Tegmark et al., *Astrophys. J.* **606**, 702 (2004).
[4] C. Deffayet, *Phys. Lett. B* **502**, 199 (2001).
[5] P. Binetruy, C. Deffayet, U. Ellewanger and D. Langlois; *Phys. Lett. B* **477** 285 (2000).
[6] R. Maartens; *astro-ph/0602415*.
[7] S. Capozziello, V.F. Cardone, S. Carloni and A. Troisi, *Int. J. Mod. Phys. D* **12**, 1969 (2003).
[8] R. G. Clowes, K. A. Harris, S. Raghunathan, L. E. Campusano, I. K. Soechting and M. J. Graham, *Mon. Not. Roy. Astron. Soc.* **429**, 2910 (2013). [arXiv:1211.6256 [astro-ph.CO]].
[9] G. Lemaitre, *Gen. Rel. Grav.* **29** (1997) 641 [*Annales Soc. Sci. Brux. Ser. I Sci. Math. Astron. Phys. A* **53** (1933) 51]. R. C. Tolman, *Proc. Nat. Acad. Sci.* **20** (1934) 169 [*Gen. Rel. Grav.* **29** (1997) 935]. H. Bondi, *MNRAS* **107**, 410 (1947).
[10] C. Clarkson, *Comptes Rendus Physique* **13** (2012) 682 [arXiv:1204.5505 [astro-ph.CO]].
[11] M. Blomqvist and E. Mortsell, *astro-ph/0909.4723*.
[12] M. Kunz and D. Sapone, *Phys. Rev. Lett.* **98**, 121301 (2007).
[13] D. Sapone, *Int. J. Mod. Phys. A* **25**, 5253-5331 (2010) [arXiv:1006.5694 [astro-ph.CO]].
[14] C. Clarkson, B. Bassett and T. Hui-Ching Lu, *Phys. Rev. Lett.* **101** 011301 (2008).
[15] D. L. Wiltshire, *New J. Phys.* **9** (2007) 377 [gr-qc/0702082].
[16] D. L. Wiltshire, *Phys. Rev. D* **80** (2009) 123512 [arXiv:0909.0749 [astro-ph.CO]].
[17] T. Buchert and S. Räsänen, *Ann. Rev. Nucl. Part. Sci.* **62** (2012) 57 [arXiv:1112.5335 [astro-ph.CO]].
[18] A. Avgoustidis, L. Verde and R. Jimenez, *JCAP* **0906** (2009) 012 [arXiv:0902.2006 [astro-ph.CO]].
[19] A. Shafieloo and C. Clarkson, *Phys. Rev. D* **81** (2010) 083537 [arXiv:0911.4858 [astro-ph.CO]].
[20] S. Räsänen, *JCAP* **0902** (2009) 011 [arXiv:0812.2872 [astro-ph]].
[21] S. February, J. Larena, M. Smith and C. Clarkson, *Mon. Not. Roy. Astron. Soc.* **405** (2010) 2231 [arXiv:0909.1479 [astro-ph.CO]].
[22] C. Boehm and S. Räsänen, *JCAP* **1309** (2013) 003 [arXiv:1305.7139 [astro-ph.CO], arXiv:1305.7139].
[23] M. Lavinto, S. Räsänen and S. J. Szybka, *JCAP* **1312** (2013) 051 [arXiv:1308.6731 [astro-ph.CO]].
[24] J. Larena, J. -M. Alimi, T. Buchert, M. Kunz and P. -S. Corasaniti, *Phys. Rev. D* **79** (2009) 083011 [arXiv:0808.1161 [astro-ph]].
[25] E. Mortsell and J. Jonsson, arXiv:1102.4485 [astro-ph.CO].
[26] S. Räsänen, arXiv:1312.5738 [astro-ph.CO].
[27] C. Clarkson, *Comptes Rendus Physique* **13** (2012) 682 [arXiv:1204.5505 [astro-ph.CO]].
[28] V. Marra and A. Notari, *Class. Quant. Grav.* **28** (2011) 164004 [arXiv:1102.1015 [astro-ph.CO]].
[29] R. Jimenez, L. Verde, T. Treu and D. Stern, *Astrophys. J.* **593** (2003) 622 [astro-ph/0302560].
[30] J. Simon, L. Verde and R. Jimenez, *Phys. Rev. D* **71** (2005) 123001 [astro-ph/0412269].
[31] M. Kowalski *et al.* [Supernova Cosmology Project Collaboration], *Astrophys. J.* **686** (2008) 749 [arXiv:0804.4142 [astro-ph]].
[32] R. Amanullah, C. Lidman, D. Rubin, G. Aldering, P. Astier, K. Barbary, M. S. Burns and A. Conley *et al.*, *Astrophys. J.* **716** (2010) 712 [arXiv:1004.1711 [astro-ph.CO]].
[33] D. Stern, R. Jimenez, L. Verde, M. Kamionkowski and S. A. Stanford, *JCAP* **1002** (2010) 008 [arXiv:0907.3149 [astro-ph.CO]].
[34] E. Gaztanaga, A. Cabre and L. Hui, *Mon. Not. Roy. Astron. Soc.* **399** (2009) 1663 [arXiv:0807.3551 [astro-ph]].
[35] A. G. Riess, L. Macri, S. Casertano, M. Sosey, H. Lampeitl, H. C. Ferguson, A. V. Filippenko and S. W. Jha *et al.*, *Astrophys. J.* **699** (2009) 539 [arXiv:0905.0695 [astro-ph.CO]].
[36] M. Hicken, W. M. Wood-Vasey, S. Blondin, P. Challis, S. Jha, P. L. Kelly, A. Rest and R. P. Kirshner, *Astrophys. J.* **700** (2009) 1097 [arXiv:0901.4804 [astro-ph.CO]].
[37] E. Komatsu *et al.* [WMAP Collaboration], *Astrophys. J. Suppl.* **180** (2009) 330 [arXiv:0803.0547 [astro-ph]].

- [38] W. J. Percival *et al.* [SDSS Collaboration], *Mon. Not. Roy. Astron. Soc.* **401** (2010) 2148 [arXiv:0907.1660 [astro-ph.CO]].
- [39] Y. Wang and P. Mukherjee, *Phys. Rev. D* **76** (2007) 103533 [astro-ph/0703780].
- [40] R. Laureijs, *et al.*, arXiv:0912.0914 [astro-ph.CO].
- [41] R. Laureijs, J. Amiaux, S. Arduini, J. -L. Augueres, J. Brinchmann, R. Cole, M. Cropper and C. Dabin *et al.*, arXiv:1110.3193 [astro-ph.CO].
- [42] M. Moresco *et al.*, *JCAP* **1208**, 006 (2012) [arXiv:1201.3609 [astro-ph.CO]].
- [43] <http://supernova.lbl.gov/Union/>.
- [44] N. Suzuki *et al.*, *Astrophys. J.* **746**, 85 (2012) [arXiv:1105.3470 [astro-ph.CO]].
- [45] A. G. Riess, L. Macri, S. Casertano, H. Lampeitl, H. C. Ferguson, A. V. Filippenko, S. W. Jha and W. Li *et al.*, *Astrophys. J.* **730** (2011) 119 [Erratum-ibid. **732** (2011) 129] [arXiv:1103.2976 [astro-ph.CO]].
- [46] P. A. R. Ade *et al.* [Planck Collaboration], arXiv:1303.5076 [astro-ph.CO].
- [47] S. Nesseris and J. Garcia-Bellido, *Phys. Rev. D* **88**, 063521 (2013), [arXiv:1306.4885 [astro-ph.CO]].
- [48] <http://www.uam.es/savvas.nesseris/codes.html>
- [49] D. Huterer and A. Cooray, *Phys. Rev. D* **71**, 023506 (2005). [astro-ph/0404062].
- [50] C. Bogdanos and S. Nesseris, *JCAP* **0905**, 006 (2009) [arXiv:0903.2805 [astro-ph.CO]].
- [51] S. Nesseris and A. Shafieloo, *Mon. Not. Roy. Astron. Soc.* **408**, 1879 (2010) [arXiv:1004.0960 [astro-ph.CO]].
- [52] S. Nesseris and J. Garcia-Bellido, *JCAP* **1211**, 033 (2012) [arXiv:1205.0364 [astro-ph.CO]].
- [53] A. Lewis, A. Challinor and A. Lasenby, *Astrophys. J.* **538** (2000) 473 [astro-ph/9911177].
- [54] "H. J. Seo, D. J. Eisenstein", *Ap. J.* **598**, 720 (2003).
- [55] L. Amendola, C. Quercellini, E. Giallongo, *MNRAS* **357**, 429 (2005).
- [56] D. Sapone, L. Amendola, astro-ph/0709.2792.
- [57] A. Orsi, C. M. Baugh, C. G. Lacey, A. Cimatti, Y. Wang and G. Zamorani, arXiv:0911.0669 [astro-ph.CO].
- [58] E. Majerotto, L. Guzzo, L. Samushia, W. J. Percival, Y. Wang, S. de la Torre, B. Garilli and P. Franzetti *et al.*, arXiv:1205.6215 [astro-ph.CO].
- [59] B. Garilli *et al.*, in preparation.
- [60] Amendola, L and Tsujikawa S. **2010**), "*Dark Energy: Theory and Observations*", Cambridge University Press, First Edition.
- [61] J. Garcia-Bellido and T. Haugboelle, *JCAP* **0909**, 028 (2009). [arXiv:0810.4939 [astro-ph]].
- [62] J. A. G. Duley, M. A. Nazer and D. L. Wiltshire, *Class. Quant. Grav.* **30** (2013) 175006 [arXiv:1306.3208 [astro-ph.CO]].
- [63] W. Valkenburg, V. Marra and C. Clarkson, *Mon. Not. Roy. Astron. Soc.* **438** (2014) L6 [arXiv:1209.4078 [astro-ph.CO]].
W. Valkenburg, M. Kunz and V. Marra, arXiv:1302.6588 [astro-ph.CO].